Journal of Oceanography
https://doi.org/10.1007/s10872-021-00616-3

SPECIAL SECTION: ORIGINAL ARTICLE

Coastal Ecosystem Change in Asia: Hypoxia, Eutrophication, and Nutrient Conditions

# Hypoxia in the Upper Gulf of Thailand: Hydrographic observations and modeling

**Akihiko Morimoto[1] · Yoshihisa Mino[2] · Anukul Buranapratheprat[3] · Atsushi Kaneda[4] · Siraporn Tong-U-Dom[3] · Kalanyu Sunthawanic[5] · Xiaojie Yu[6] · Xinyu Guo[1]**

Received: 3 April 2021 / Revised: 29 July 2021 / Accepted: 12 August 2021
© The Oceanographic Society of Japan and Springer Nature Singapore Pte Ltd. 2021

**Abstract**
We conducted hydrographic observations throughout the year to investigate seasonal variations of the hypoxic water mass distribution in the Upper Gulf of Thailand (UGoT). Hypoxic water masses were observed from June to November, with half of the UGoT occupied by hypoxic water in September. A hypoxic water mass appeared in the northeastern part of the UGoT in June and August, and moved westward over time. Low-salinity surface water moved from east to west as the rotational direction of surface circulation shifted with the reversal of monsoon winds. Westward movement of low-salinity water causes strong stratification in the northwestern part of the UGoT, leading to severe hypoxia. Numerical experiments showed high dissolved oxygen consumption rates around and offshore of river mouths, where hypoxic water is generated. This finding suggests that hypoxic water masses are transported to the south by physical processes. We examined how flooding affects hypoxic water mass formation. The volume of hypoxia in a flood year was approximately 2.5 times greater than in a normal year. In addition, hypoxia occurred in the dry season and extensive hypoxia was observed in the year after flooding. These results suggest that the hypoxic water mass persists for a long time after flooding.

**Keywords** Hypoxia · Upper Gulf of Thailand · Ecosystem model

## 1 Introduction

Hypoxia, which is often defined as a dissolved oxygen (DO) concentration in seawater of less than 2 mg $l^{-1}$ (Diaz 2001; Kemp et al. 2009) has occurred since the 1960s in the costal seas of developed countries such as the United States and Japan, and in European countries, due to enormous nutrient and organic matter inputs via rivers in association with rapid economic growth (Diaz 2001; Capet et al. 2013; Carstensen et al. 2014; Li et al. 2016; Breitburg et al. 2018; Rabalais and Turner 2019). Although substantial efforts have been made over time to reduce hypoxia in many countries, the environmental problem of hypoxia has not yet been solved (Diaz and Rosenberg 2008; Kemp et al. 2009). For example, after an eutrophication problem arose in the Seto Inland Sea in Japan, sewage systems were installed and total volume control was applied for nitrogen and phosphorus. As a result, nutrient concentrations in the Seto Inland Sea decreased. However, hypoxia continued to occur every summer in Osaka Bay, which is located in the eastern part of the Seto Inland Sea (Nakajima and Fujiwara 2007). Only Dokai Bay in Japan, which is a very narrow and small embayment, showed improvement from hypoxic conditions (Yanagi and Yamada 2014). These findings demonstrate that it is difficult for the marine environment to recover from hypoxic conditions. Recently, hypoxia has also occurred in developing

✉ Akihiko Morimoto
morimoto.akihiko.cl@ehime-u.ac.jp

1 Center for Marine Environmental Studies, Ehime University, 2-5 Bunkyo-Cho, Matsuyama, Ehime 790-8577, Japan

2 Institute for Space-Earth Environmental Research, Nagoya University, Nagoya, Aichi, Japan

3 Department of Aquatic Science, Faculty of Science, Burapha University, Chonburi, Thailand

4 Faculty of Marine Science and Technology, Fukui Prefectural University, Obama, Fukui, Japan

5 Department of Mathematics, Faculty of Science, Mahidol University, Bangkok, Thailand

6 Key Laboratory of Marine Environment and Ecology, Mistry of Education, Ocean University China, Qingdao, China

Published online: 24 August 2021

countries in Southeast Asia due to rapid economic growth (e.g., Jacinto et al. 2011; Sotto et al. 2014; Hayami et al. 2020). Hypoxia has become a worldwide environmental problem affecting coastal seas. However, reports of hypoxia in Southeast Asia are scarce, likely due to a lack of observed data. In terms of hypoxia, coastal marine environments in Southeast Asia might be more severely impacted than first thought. Tropical regions might be more vulnerable to hypoxia than temperate regions because the solubility of oxygen is lower due to higher water temperatures throughout the year (Altieri and Gedan 2015), and because vertical mixing is weaker due to a lack of winter cooling. In addition, during the rainy season, a large amount of fresh water with high nutrient levels flows into coastal seas, leading to strong density stratification (Buranapratheprat et al. 2008a) that in turn might lead to red tides and hypoxia (Lirdwitayaprasit et al. 2006; Buranapratheprat et al. 2009).

The Upper Gulf of Thailand (UGoT) borders the capital city of Thailand (Bangkok). The width and length of the UGoT are approximately 100 km, and the UGoT is a very shallow bay with a maximum water depth of less than 40 m. Five rivers, the Bangpakong, Chaopraya, Thachin, Maeklong, and Phet Chaburi, supply fresh water and materials such as nutrients and organic matter to the UGoT (Fig. 1). The largest river is the Chaopraya River (mean discharge of 718 $m^3\ s^{-1}$), which passes through Bangkok city. Although the UGoT is a high-productivity coastal sea with high fish production, the marine environment of the UGoT has recently deteriorated due to large inputs of organic and inorganic matter from its five inflowing rivers. Mass mortality of shellfish and fish occurs every year from August to early October along the eastern coast of the UGoT. This mortality might be due to red tides and hypoxia. Morimoto et al. (2013) reported that hypoxia and anoxia occurred in the river mouth area of the Bangpakong River from late September to October. In addition, they suggested that a water mass with low DO was transported from another area to the Bangpakong River estuary, indicating that hypoxia occurs over a large area of the UGoT. Chongprasith and Srineth (1998) and Cheevaporn and Menasveta (2003) both reported eutrophication throughout the entire UGoT. Massive quantities of nutrients from rivers comparing to those in developed countries are transported along the UGoT coast via a clockwise circulation pattern in summer and an anti-clockwise pattern in winter (Buranapratheprat et al. 2002). The northern part of the UGoT has a content of high chlorophyll-*a*, which moves westward or eastward according to the season (Buranapratheprat et al. 2008a, b). It has been suggested that hypoxia or anoxia occur across large areas of the UGoT, but few data show the seasonal variations of DO concentration across the whole UGoT.

In the present study, we reveal seasonal variations of DO concentration across the entire UGoT based on hydrographic observations, and investigate the factors that generate hypoxia. Then, we describe a coupled physical-ecosystem model developed to clarify the spatial and temporal

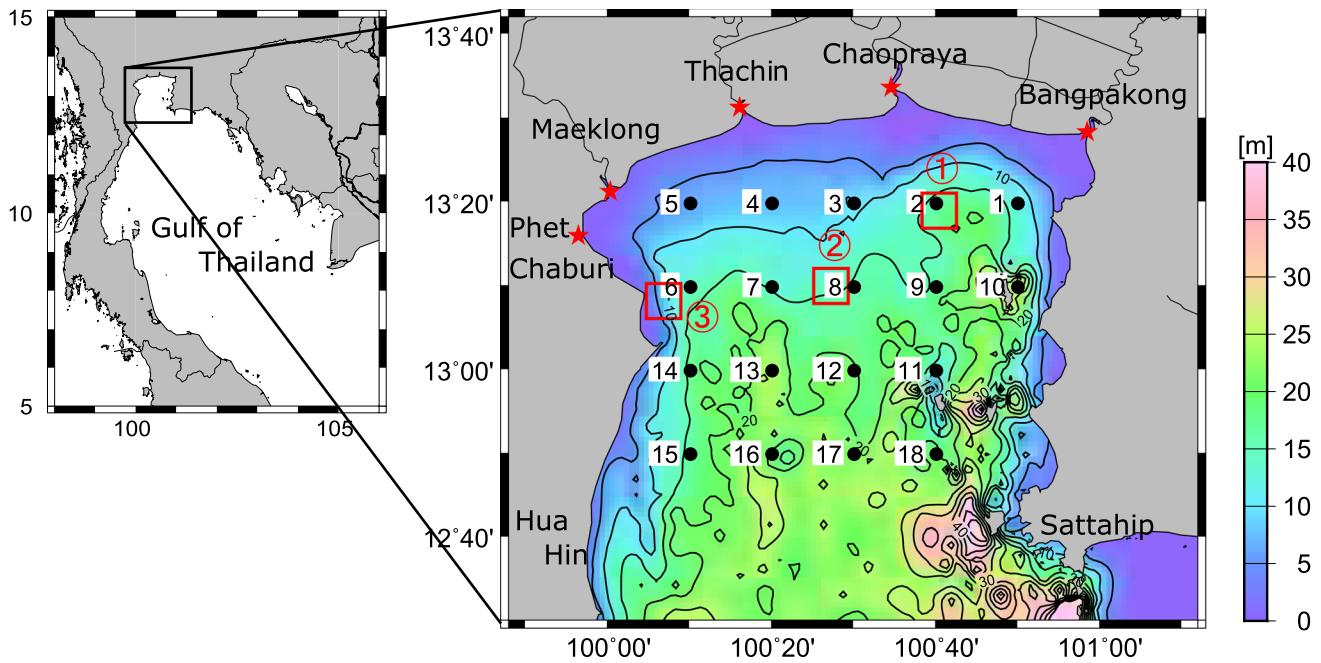


**Fig. 1** Bathymetry in the Upper Gulf of Thailand. Black dots denote hydrographic observation stations and red stars denote observation point in the rivers. Temporal variations in DO, DO consumption rate, PON concentration, vertical integrated chlorophyll-a and intensity of stratification shown in Figs. 11, 12, and 13 are examined in three red square areas (colour figure online)

variations of hypoxia in the UGoT. In addition, we examine the influence of river discharge changes on the volume and horizontal distribution of the hypoxic water mass, as flooding occurs in some years and river discharge has shown a recent increasing trend.

## 2 Observations and numerical modeling

### 2.1 Hydrographic observations

We conducted seven sets of hydrographic observations, from August 2014 to June 2015, by the research vessel of Kasetsart University. Dates of the observations and moon phase are shown in Table 1. We sampled 18 stations in the UGoT (Fig. 1), using a RINKO Profiler (JFE Advantec Co. Ltd.) for measurement of water temperature, salinity, DO, fluorescence, and turbidity. The vertical interval of the data was 0.1 m at each station. We collected water samples 1 m below the sea surface and 1 m above the bottom for measurement of DO, chlorophyll-*a*, and nutrient concentrations (nitrate, nitrite, ammonia, phosphate, and silicate). The DO concentrations of water samples were measured using the Winkler method. Water samples for chlorophyll-*a* measurement were filtered onto 40-mm Whatman GF/F filters and then immersed in *N*,*N*-dimethylformamide for extraction. The chlorophyll-*a* concentration was analyzed with a Turner Designs Model 10 fluorometer. DO and fluorescence values measured with the RINKO Profiler were corrected according to the measured values of DO and chlorophyll-*a* derived from water samples, respectively. The same types of observations were conducted at the mouths of five rivers (Fig. 1) a few days before each hydrographic observation, as shown in Table 1. We collected water samples at 1 m below the surface and 1 m above the bottom for measurement of DO, chlorophyll-*a*, and nutrient concentrations in river water.

### 2.2 Physical and ecosystem numerical models

To reproduce physical properties such as current, water temperature, and salinity during the observation period from August 2014 to June 2015, we developed a three-dimensional sigma-coordinate physical model based on the Princeton Ocean Model (Blumberg and Mellor 1987; Mellor 2003). The vertical and horizontal diffusivities are calculated with the momentum turbulent closure scheme (Mellor and Yamada 1982) and Smagorinsky formula (Smagorinsky 1963), respectively. The horizontal and vertical resolutions of the model are 1/120 degree latitude and longitude, and 10 sigma layers, respectively. The model domain is 99.75–101.25 E and 12.60–13.6 N (Fig. 1). The integration period of the model is from January 1, 2014, to June 30, 2015. The model configurations are similar to those reported by Yu et al. (2018), but the boundary conditions differ as follows. Sea-level variation is enforced at the southern end of the model domain to reproduce tides and tidal currents. We consider four main tidal constituents: $M_2$, $S_2$, $O_1$, and $K_1$. The harmonic constants of these four tidal constituents are determined at Sattahip and Hua Hin tide gauge stations, which are located in the southern part of the UGoT (Fig. 1), and the harmonic constants were linearly interpolated into grids with the southern end of the domain treated as an open boundary condition. Daily wind stresses during the integration period were applied at the sea surface and calculated from wind data observed at three stations around the UGoT. Daily net heat flux obtained from the National Center for Environmental Prediction (NCEP) from January 2014 to June 2015 was used as a sea surface boundary condition. We considered river discharge from five rivers, namely the Bangpakong, Chaopraya, Thachin, Maeklong, and Phet Chaburi. Monthly averaged river discharge data during the integration period were used (Fig. 4). Vertical profiles of water temperature, salinity, and the north–south component of the monthly mean current were set at the southern end of the model domain as open boundary conditions, using values derived from the diagnostic model results of Tong-U-Dom et al. (2017).

We coupled the physical model described above with a simple ecosystem model to investigate the hypoxia in the UGoT. The ecosystem model is a nutrient-phytoplankton-zooplankton-detritus (NPZD) model (e.g., Onitsuka et al. 2007; Buranapratheprat et al. 2008a, b) with DO processes added (Kim et al. 2019) (Fig. 2). Variables in the model include nutrients, dissolved inorganic nitrogen (DIN), dissolved inorganic phosphorus (DIP), phytoplankton, zooplankton, detritus, and DO. Details of the NPZD model, such as its governing equations, were provided by Onitsuka et al. (2007) and Kim et al. (2019), and the biogeochemical parameters of the NPZD model applied here are shown in Table 2. As lateral boundary conditions, DIN, DIP, chlorophyll-*a*, and detritus were supplied from five river mouths and an open boundary at the southern end of the model domain based on observed concentrations. However, no detritus data were available. Therefore, we assumed that

**Table 1** Observation days and moon phase of observed day

| | Observation date | Moon phase |
|---|---|---|
| 1 | August 8–10, 2014 | 12.2–14.2 |
| 2 | September 22–24, 2014 | 27.5–29.5 |
| 3 | November 5–7, 2014 | 12.2–14.2 |
| 4 | December 18–20, 2014 | 25.6–27.6 |
| 5 | February 16–18, 2015 | 26.6–28.6 |
| 6 | April 2–4, 2015 | 12.7–14.7 |
| 7 | June 14–16, 2015 | 26.9–28.9 |

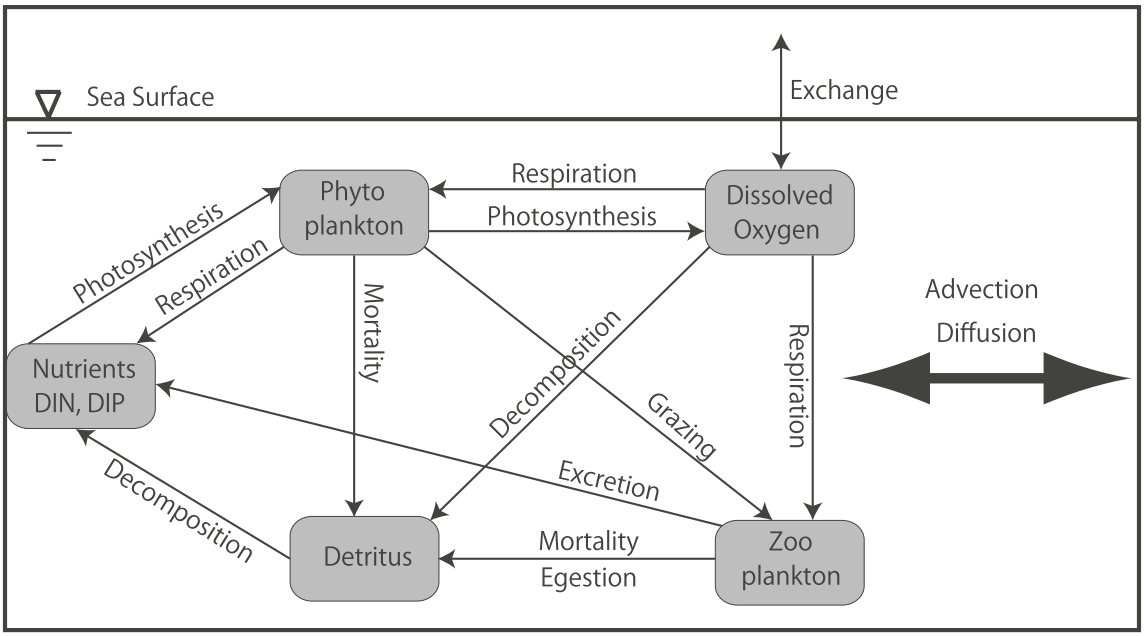


**Fig. 2** Configuration of ecosystem model

**Table 2** Biogeochemical parameters in the ecosystem model

| Definition | Value | Unit |
|---|---|---|
| Maximum photosynthetic rate of phytoplankton at 0 ℃ | 0.75 | $day^{-1}$ |
| Half saturation constant of phytoplankton for DIN | 3 | mmol N $m^{-3}$ |
| Half saturation constant of phytoplankton for DIP | 0.1 | mmol N $m^{-3}$ |
| Temperature coefficient for the photosynthetic rate | 0.0693 | $℃^{-1}$ |
| Optimum light intensity for phytoplankton | 80 | W $m^{-2}$ |
| Light dissipation coefficient of seawater | 0.04 | $m^{-1}$ |
| Self-shading coefficient | 0.054 | $m^2$ mmol $N^{-1}$ |
| Respiration rate of phytoplankton at 0 ℃ | 0.05 | $day^{-1}$ |
| Temperature coefficient for respiration | 0.0519 | $℃^{-1}$ |
| Mortality rate of phytoplankton at 0 ℃ | 0.03 | $m^3$ mmol $N^{-1}$ $day^{-1}$ |
| Temperature coefficient for phytoplankton mortality | 0.0693 | $℃^{-1}$ |
| Maximum grazing rate of zooplankton at 0 ℃ | 0.5 | $day^{-1}$ |
| Ivelev constant | 1.4 | $m^3$ mmol $N^{-1}$ |
| Threshold value for grazing | 0.043 | $℃^{-1}$ |
| Temperature coefficient for grazing | 0.0693 | $℃^{-1}$ |
| Assimilation efficiency of zooplankton | 0.7 | |
| Growth efficiency of zooplankton | 0.3 | |
| Zooplankton mortality rate at 0℃ | 0.06 | $m^3$ mmol $N^{-1}$ $day^{-1}$ |
| Temperature coefficient for zooplankton mortality | 0.0693 | $℃^{-1}$ |
| Decomposition rate of detritus at 0 ℃ | 0.08 | $day^{-1}$ |
| Temperature coefficient of detritus for decomposition | 0.0693 | $℃^{-1}$ |
| Sinking velocity of detritus | 1.5 | m $day^{-1}$ |
| Ratio of carbon to chlorophyll-*a* | 50 | |
| Redfield ratio of *C*:*N*:*P* | 106:16:1 | |

the concentration of detritus is 20% of the chlorophyll-*a* concentration.

## 3 Results

### 3.1 Seasonal variations in observed bottom DO, surface salinity, and surface chlorophyll-*a*

Horizontal distributions of observed DO concentration at 1 m above the bottom, surface salinity, and surface chlorophyll-*a* at seven hydrographic observation time points from August 2014 to June 2015 are shown in Fig. 3. We did not plot water temperature because the horizontal gradient of water temperature is small and vertically homogeneous at each station throughout the year. Monthly river discharges from each of the five rivers and total discharge are shown in Fig. 4. In the present study, a DO concentration less than 2 mg $l^{-1}$ is defined as hypoxia, with reference to Diaz (2001) and Kemp et al. (2009).

Hypoxia (< 2 mg $l^{-1}$) occurred in the bottom layer offshore of the mouth of the Chaopraya River in August 2014. The minimum DO value was 1.2 mg $l^{-1}$ at station 2. Surface salinity less than 31.0 psu occurred in the northeastern part of the UGoT, offshore of the Bangpakong and Chaopraya rivers. Discharge of the Bangpakong and Chaopraya rivers increased at the start of the rainy season. Although discharge of the Chaopraya River was twice as high as that of the Bangpakong River, the lowest salinity was observed off the Bangpakong River mouth. This suggests that freshwater supplied from the Chaopraya River is transported eastward by surface currents. Surface chlorophyll-*a* was nearly constant, at approximately 1 mg $m^{-3}$, across the whole UGoT.

In September 2014, a hypoxic water mass occupied half of the total area of the UGoT, and the DO concentration was less than 1 mg $l^{-1}$ off the mouth of the Chaopraya River; anoxic water with a DO concentration of zero was observed at station 3. Surface salinity became lower than in August. The lowest salinity was observed in the northeastern part of the UGoT, as in August. The surface salinities at stations 1 and 2 were 20.5 and 20.9 psu, respectively. A water mass of more than 32.0 psu was present at the bay mouth of the UGoT. The discharge of the Chaopraya River in September was more than 600 $m^3$ $s^{-1}$, which was 3 times larger than the discharge of the Bangpakong River (Fig. 4a). Nevertheless, the lowest salinity was from the Bangpakong River, as in August. Surface chlorophyll-*a* concentrations in the northern part of the UGoT were higher than in the southern part. The maximum chlorophyll-*a* concentration was 28.3 mg $m^{-3}$ at station 4. Although the chlorophyll-*a* concentration was relatively high (10.4 mg $m^{-3}$) at the mouth of the Bangpakong River, where surface salinity was lowest, the surface chlorophyll-*a* distribution pattern did not generally correspond to that of surface salinity. Moreover, the bottom DO (hypoxia), surface salinity, and surface chlorophyll-*a* distribution patterns all differed.

In November 2014, hypoxic water masses were observed in the northwestern part of the UGoT. The DO concentrations at stations 4–6 were 0 mg $l^{-1}$. Meanwhile, the hypoxia off the Bangpakong River observed in September disappeared. The distribution pattern of surface salinity in November differed markedly from that in September, with the lowest salinity water mass being located in the northwestern part of the UGoT and salinity contour lines trending north–south. This finding suggests that water masses originating outside the UGoT intruded into the UGoT from the eastern part of the bay mouth, and water with lower salinity was transported to the west. Surface chlorophyll-*a* was low (< 2 mg $m^{-3}$) in the eastern part of the UGoT, where surface salinity was high, and chlorophyll-*a* was high (> 3.5 mg $m^{-3}$) in the western part, where surface salinity was low. The distribution of hypoxic water masses appears to correspond to the area of low surface salinity and high surface chlorophyll-*a*.

No hypoxic water masses were observed in December 2014, February 2015 or April 2015, when bottom DO concentrations were above 5 mg $l^{-1}$, and surface chlorophyll-*a* concentrations were higher than in December 2014 or April 2015 near the coast. The chlorophyll-*a* distribution pattern in December 2014 was similar to that in November. During these months, surface salinity was relatively high, as river discharges were smaller (Fig. 4a). Moreover, stratification was weak in these periods due to strong winds during the dry season. In June 2015, a hypoxic water mass again appeared off the Chaopraya River; the DO concentration at station 2 was 1.5 mg $l^{-1}$. As river discharge was not large at this time, surface salinity in June was relatively high throughout the UGoT. Surface chlorophyll-*a* concentrations were higher in the northern than southern part, with a maximum concentration of 5.4 mg $m^{-3}$ at station 3.

Zonal sections of DO and density at the northern observation stations (stations 1–5) from June to November, when hypoxia occurred (Fig. 3), are shown in Fig. 5. Weak stratification was recorded at stations 2 and 5 in June, and a water mass with low DO (< 3 mg $l^{-1}$) occurred only at station 2. In August, the water column was vertically homogenous in the western part, and weak stratification was present at station 2, which had begun during the rainy season (Fig. 4a). In August, a hypoxic water mass was present only at station 2, and the distribution pattern of DO was similar to that in June. Stratification developed in September, especially in the eastern part of the UGoT, and hypoxic water masses extended from the eastern to the western part. The thickness of the hypoxic water mass at stations 2 and 3 was about 5 m, while station 4 and 5 had about 1 m and 2 m of hypoxic water, respectively.

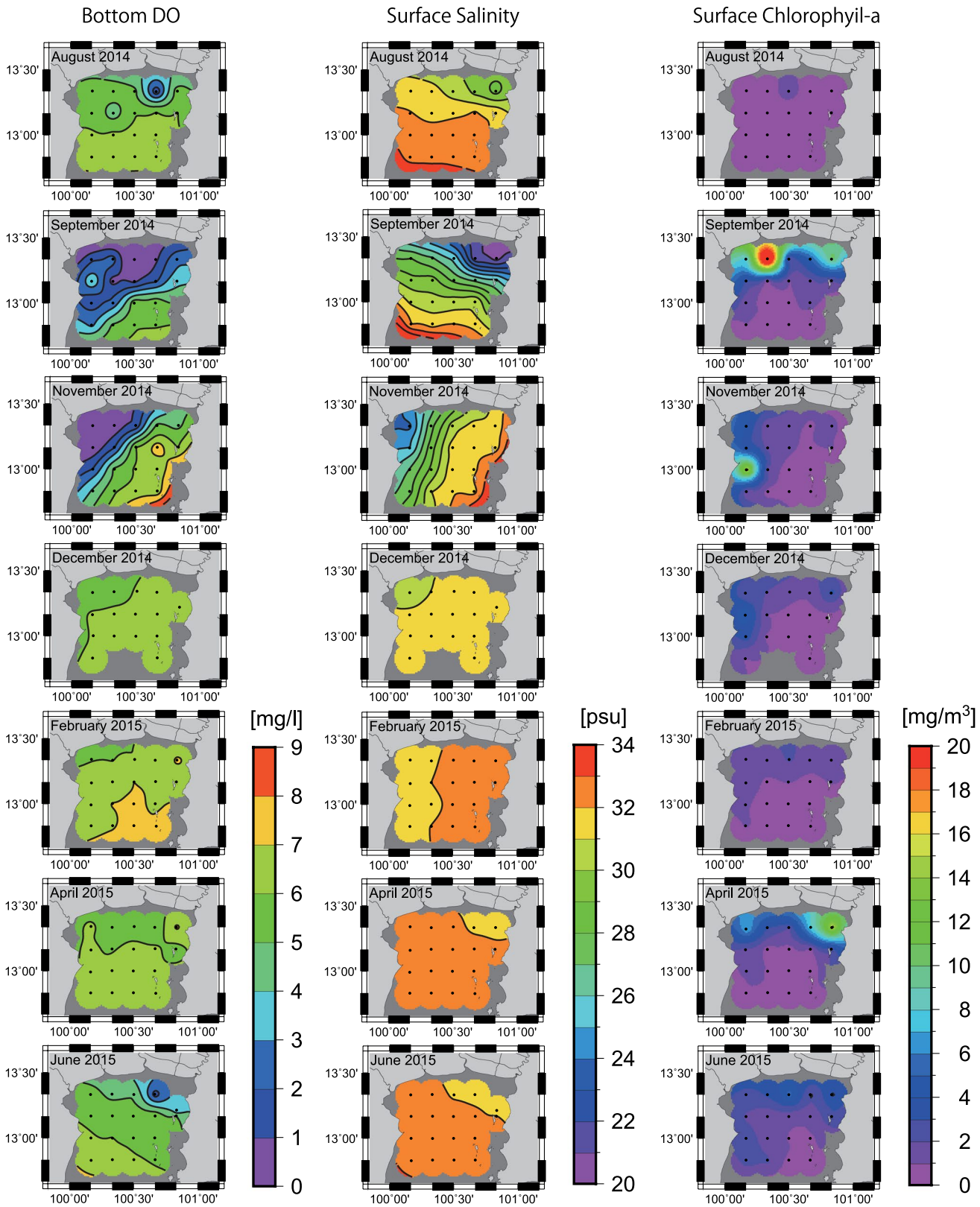


**Fig. 3** Horizontal distributions of observed DO at 1 m above the bottom, surface salinity at 1 m below the sea surface, and chlorophyll-*a* concentration at 1 m below the sea surface from August 2014 to June 2015. Black lines in the figures show isolines; every 1 mg $l^{-1}$ for bottom DO and 1 psu for surface salinity

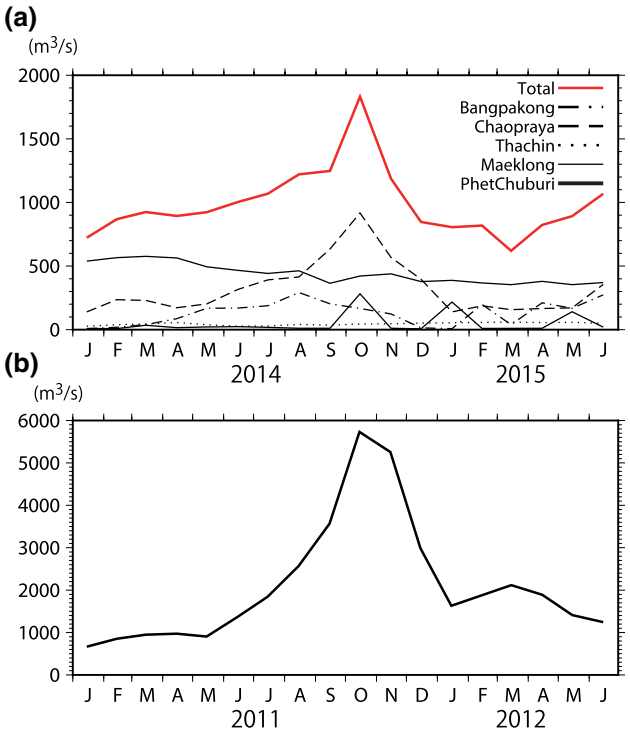


**Fig. 4** **a** Monthly mean of river discharges of five rivers shown in Fig. 1 and total discharge (red line) from January 2014 to June 2015. **b** Monthly mean of total discharge of five rivers from January 2011 to June 2012 (colour figure online)

At station 1, the lowest DO was recorded at a depth of 9 m, indicating that a low-DO water mass had intruded from another area. In November, stratification developed at stations 4 and 5, and hypoxic and anoxic water masses were observed. Surface DO was high (oversaturated) in the western part due to a high chlorophyll-*a* concentration, and DO was low at depths just below the high-DO water mass. This finding suggests that oxygen in the lower layer is consumed locally due to the decomposition of organic matter produced by phytoplankton.

## 3.2 Relationships among hypoxia, intensity of stratification and vertical supply of organic matter

In general, hypoxia occurs due to the inhibition of vertical oxygen supply under conditions of strong stratification and high supply of organic matter to the bottom layer, which occur with phytoplankton blooms in surface layer. We examined the relationships among the bottom DO concentration, intensity of stratification and chlorophyll-*a* concentration. As an index of stratification, we used the potential energy anomaly (PEA), calculated as follows:

$$\mathrm{PEA} = \frac{1}{h}\int_{-h}^{0} g\{\rho_A - \rho(z)\}z\mathrm{d}z, \quad (1)$$

where $h$ is water depth, $g$ is gravity acceleration, $\rho_A$ is vertically averaged density, and $\rho(z)$ is density at depth z. As an index of organic matter, we used the vertically averaged chlorophyll-*a* concentration (VAC). In September, PEA and bottom DO had a negative correlation coefficient of −0.42, but station 14 had low DO with weak stratification (low PEA) (Fig. 6a); the difference between surface and bottom salinities was 1.05 psu. The correlation between VAC and bottom DO in September was weak ($r = -0.24$), but a positive correlation was found under hypoxic conditions (DO < 2 mg $l^{-1}$) (Fig. 6b). As the VAC at station 14 was relatively high while PEA was low (Fig. 6a), vertical supply of organic matter might be the main driver of hypoxia at that location. In November, bottom DO had strong negative correlations with PEA and VAC (Fig. 6c, d), with correlation coefficients between bottom DO and PEA, and between bottom DO and VAC, of −0.78 and −0.76, respectively. Stations 5 and 6 had low DO (< 0.5 mg $l^{-1}$), and both PEA and VAC were high. At these stations, both low vertical supply of oxygen and high vertical supply of organic matter might reduce DO at the bottom. As PEA at station 4 was relatively low, whereas VAC was at its maximum, anoxic conditions might be generated due to high organic matter supply. At station 3, PEA was quite small (the difference between surface and bottom salinity was 0.63 psu) and VAC was not elevated; however, a hypoxic water mass was present. This indicates that the hypoxic water mass was transported from another area.

Based on these hydrographic observations, we found that hypoxia occurred from June to November in the UGoT, and that almost half of the UGoT by area was occupied by hypoxic water masses in September. Hypoxia appeared in the eastern part of the UGoT in June and August, and the hypoxic area moved westward in September and November. In general, bottom DO had negative correlations with both the intensity of stratification and VAC, and hypoxia was observed at a few stations with weak stratification and low chlorophyll-*a*. This tendency might be driven by hypoxic water masses generated in other areas that are transported by currents. To clarify the generation process and behavior of hypoxic water masses, we investigated them using a numerical model.

## 3.3 Numerical modeling results

### 3.3.1 Validation of the numerical model

Figure 7 shows the calculated and observed temporal variations in DO at 1 m above the bottom, and the salinity at 1 m below the sea surface, at stations 2, 4, and 6. At station

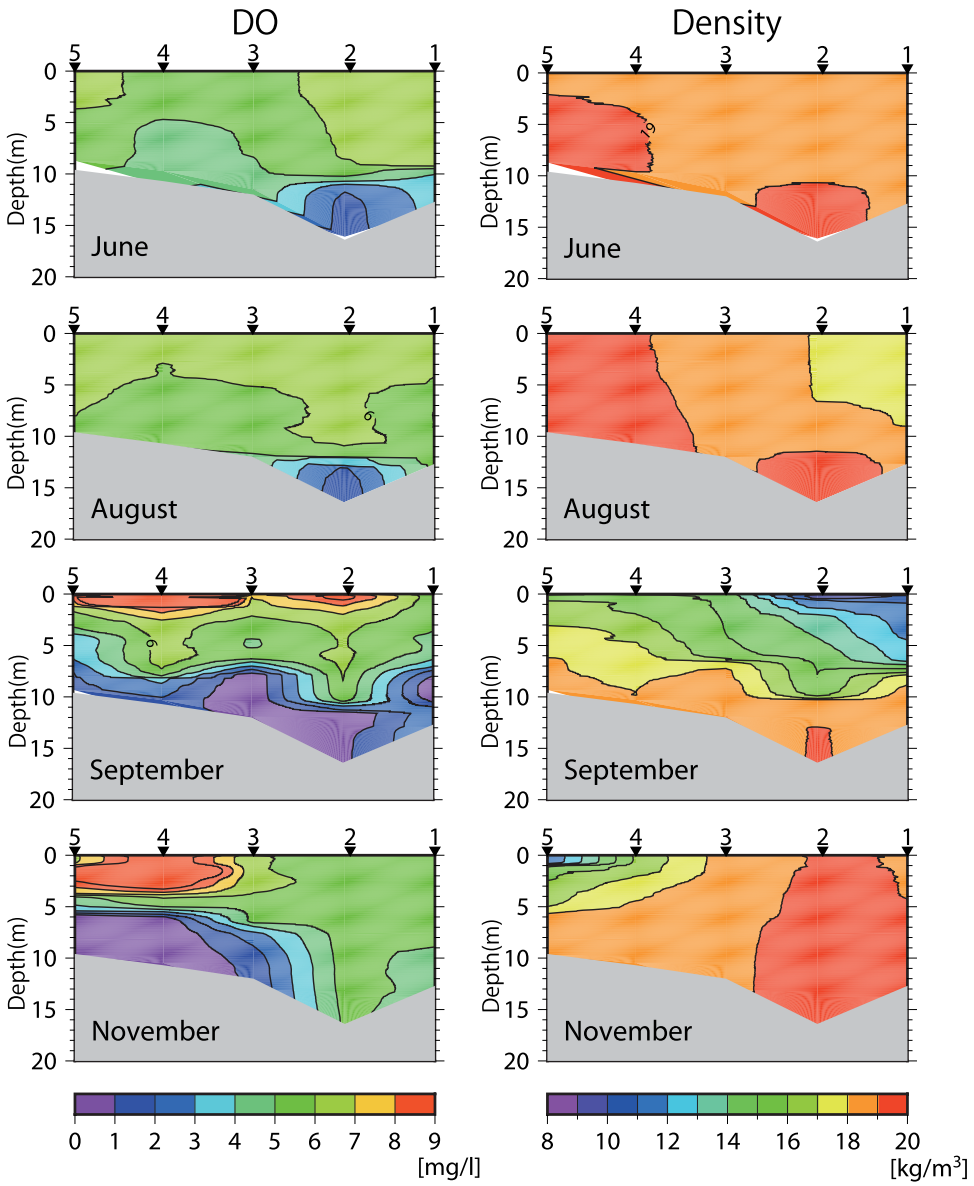


**Fig. 5** Cross section along northern coast (Station 1–5 shown in Fig. 1) of observed DO and density from June to November

2, which is located off Chaopraya River mouth, the calculated bottom DO from August to mid-September was less than 2 mg $l^{-1}$ and increased gradually from mid-September to December aside from two sudden drops (early October and mid-November). The high concentration of bottom DO continued to the end of March, after which it gradually decreased (in early May), and then increased (in May), with hypoxia occurring in June (Fig. 7a). The calculated temporal variations of bottom DO coincide with the observed variations, although large differences were present in September and November. The calculated surface salinity in August was lower than the corresponding observations, and that in September was slightly higher than the observations. The calculated surface salinity in November, December, February reproduced the observations, but the calculated surface salinities from March to June 2015 were much lower than the observed values (Fig. 7b). At station 4, located off the Thachin River mouth, the calculated bottom DO was high in August and September and suddenly decreased in October, with anoxic conditions appearing in November. After December, the high concentration of bottom DO continued until June 2015. Although the calculated and observed bottom DO differed in September, our model reproduced the observed temporal variations in bottom DO well (Fig. 7c). The calculated surface salinity at station 4 accurately reproduced the observations from September to February, but was lower than the observations in August, April, and June, as noted at station 2 (Fig. 7d). At station 6, the calculated bottom DO was high in August and September, and dropped suddenly at the end of September, with hypoxic conditions lasting until the end of November. In December, bottom DO increased, and high concentrations continued until June

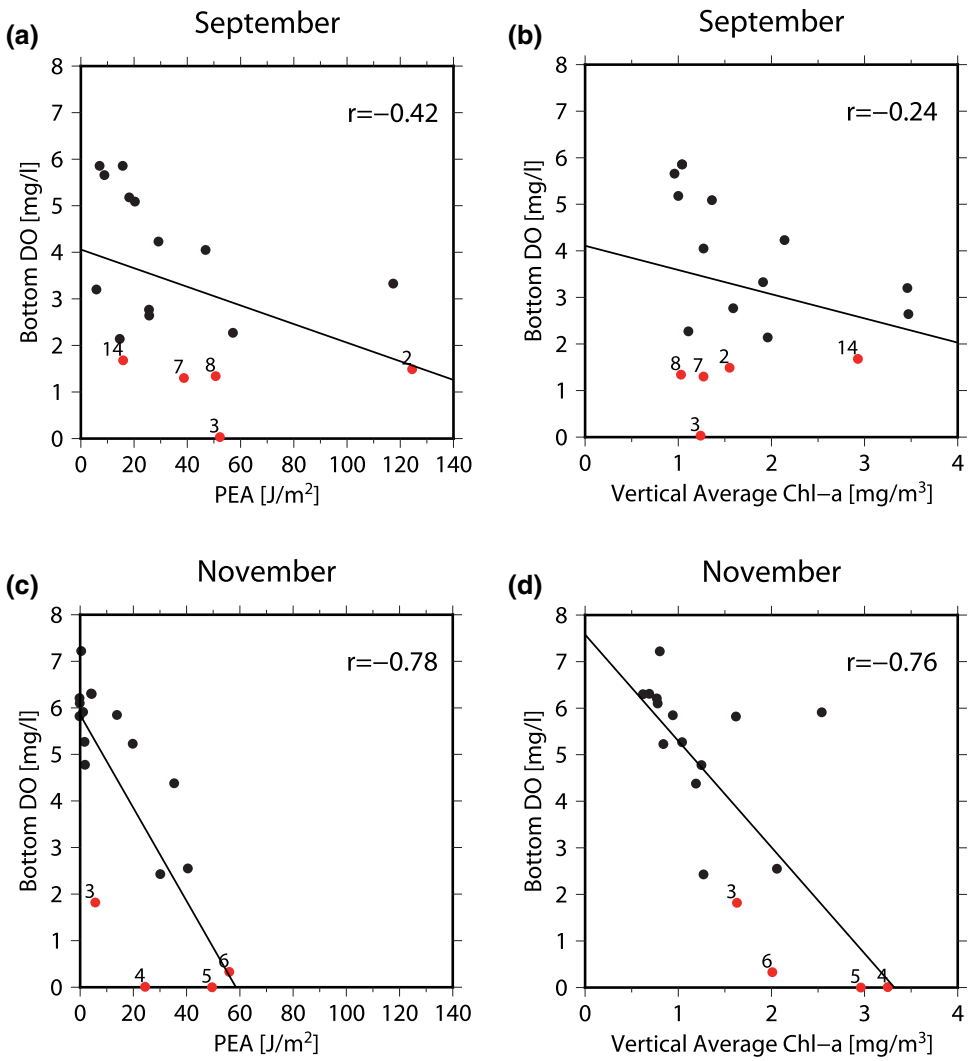


**Fig. 6** Scatter plots of intensity of stratification (PEA) versus DO concentration at 1 m above the bottom **a** in September 2014 and **c** in November 2014. Scatter plots of vertical averaged chlorophyll-*a* concentration versus DO concentration at 1 m above the bottom **b** in September 2014 and **d** in November 2014. Red dots denote DO concentration less than 2 mg $l^{-1}$ stations, and numbers denote station number shown in Fig. 1. Solid line in each figure shows regression line (colour figure online)

(Fig. 7e). The temporal variations in surface salinity were better reproduced compared to the other two stations.

Figures 8 and 9 show the calculated monthly means of surface salinity, surface chlorophyll-*a*, and bottom DO from August to November. Although surface salinity in the middle and northern parts in August was lower than the observations (Fig. 3), the surface salinity distribution in September and November coincided with the observations (Fig. 8). Surface chlorophyll-*a* in August was higher than the observations throughout the study area, whereas chlorophyll-*a* in September was reproduced well. In November, the high concentration along the western coast was reproduced accurately by the model, but the calculated surface chlorophyll-*a* concentrations in the eastern part were higher than the observations, especially near the northern coast (Fig. 9). Hypoxia around station 2 in August was reproduced. In September, the low-DO area was smaller than the observed area, especially near the northern coast. In November, the low-DO area in the northwestern part of the UGoT was reproduced. The numerical model showed seasonal movement of the hypoxic area from the eastern to the western part of the study area.

### 3.3.2 Horizontal distributions of salinity, surface currents, and bottom currents

We analyzed the physical fields from August to November 2014, when hypoxic water masses were observed. Figure 8 shows the monthly means of surface salinity, surface currents, and bottom currents from August to November 2014.

The surface salinity and current fields in August and September are quite similar. At the sea surface, eastward flow at speeds of 1–10 cm $s^{-1}$ occurs along the northern coast, while southeastward flow of about 5 cm $s^{-1}$ occurs in the southern part of the UGoT. On the other hand, bottom-layer currents flow north or northeastward at about 3 cm $s^{-1}$ to compensate for the surface current flow. The calculated surface salinity in August was much lower than observations, while that in

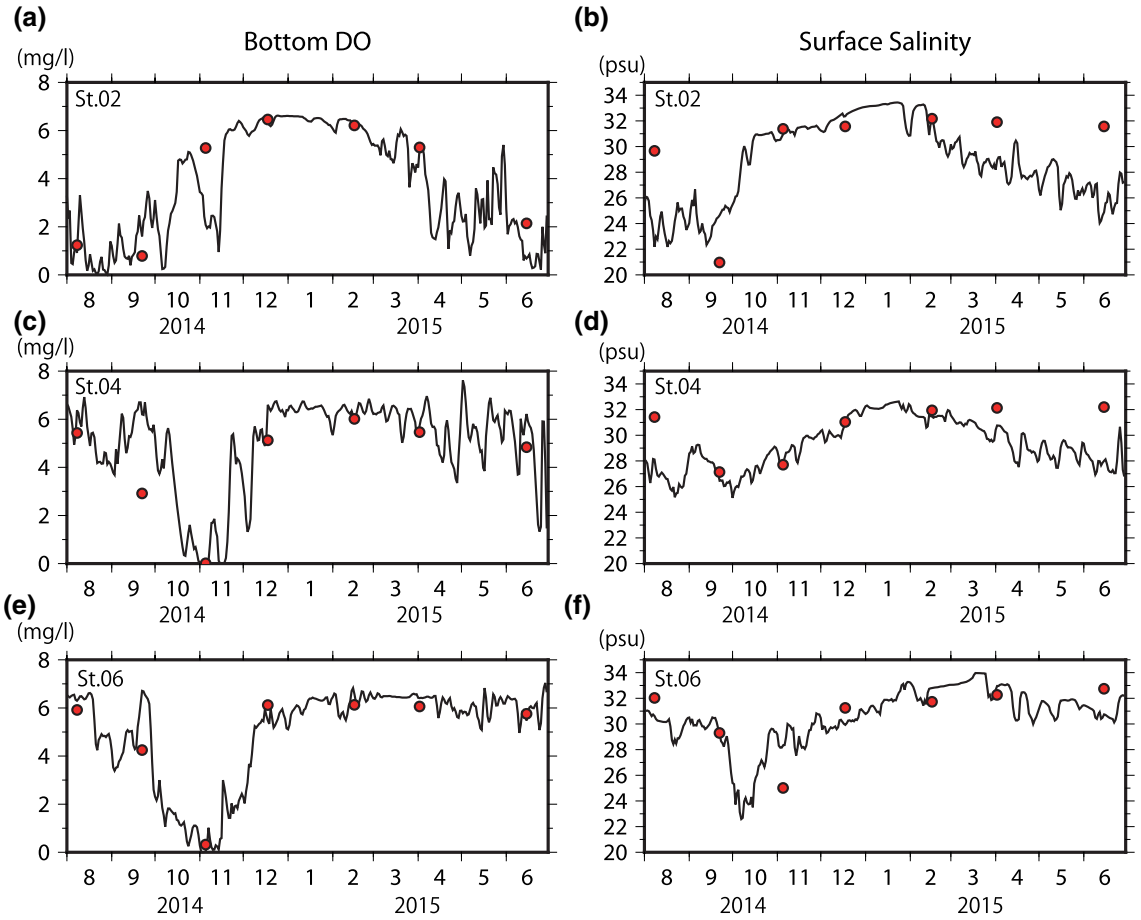


**Fig. 7** Temporal variations in DO concentration at 1 m above the bottom **a** in station 2, **c** in station 4, and **e** in station 6 and those in salinity at 1 m below the sea surface **b** in station 2, **d** in station 4, and **e** in station 6. Solid line in each figure is calculated value of numerical model and red dot in each figure is observed value (colour figure online)

September aligned well with the observations. We found that freshwater supplied from rivers is transported to the east by eastward surface flow. As a result, low-salinity water accumulates in the northeastern corner of the bay. In October, the distribution patterns of surface salinity and surface current direction differ dramatically from those in August and September due to the arrival of strong northeast winds. A surface current (speed of about 10 cm $s^{-1}$) flows southwestward in the central part of the bay, while westward flow dominates along the northern coast, and strong southward flows with a speed of about 20 cm $s^{-1}$ occur along the western coast. In the southeastern part of the bay, weak inflows are observed at the sea surface. In the bottom layer, inflow is dominant throughout the bay. Surface currents transport low-salinity water from river mouths to the west and south along the coast. As a result, salinity contours shift from northwest-southeast in September to northeast-southwest in October. The surface and bottom currents in November are similar to those in October, being dominated by strong currents along the coast. As river discharges decrease at this time (Fig. 4), the low-salinity area shrinks relative to October, while the high-salinity area becomes larger.

### 3.3.3 Temporal and spatial variations in surface chlorophyll-*a* and bottom DO

Figure 9 shows the surface chlorophyll-*a* and bottom DO from August to November 2014.

In August, high chlorophyll-*a* appeared at the mouths of the Chaopraya, Bangpakong, and Maeklong rivers. Chlorophyll-*a* was low along the western coast and southern part of the UGoT, where surface salinity tended to be high. Hypoxic water masses with DO below 2 mg $l^{-1}$ occurred at the mouths of the Bangpakong and Chaopraya rivers, and along the eastern coast, and the lowest DO (< 1 mg $l^{-1}$) was observed off the Chaopraya River. In September, surface chlorophyll-*a* was relatively high (> 10 mg $m^{-3}$) along the northern coast, and the area of lower chlorophyll-*a* expanded in the eastern part relative to August. The bottom DO distribution in September exhibited the same pattern as that

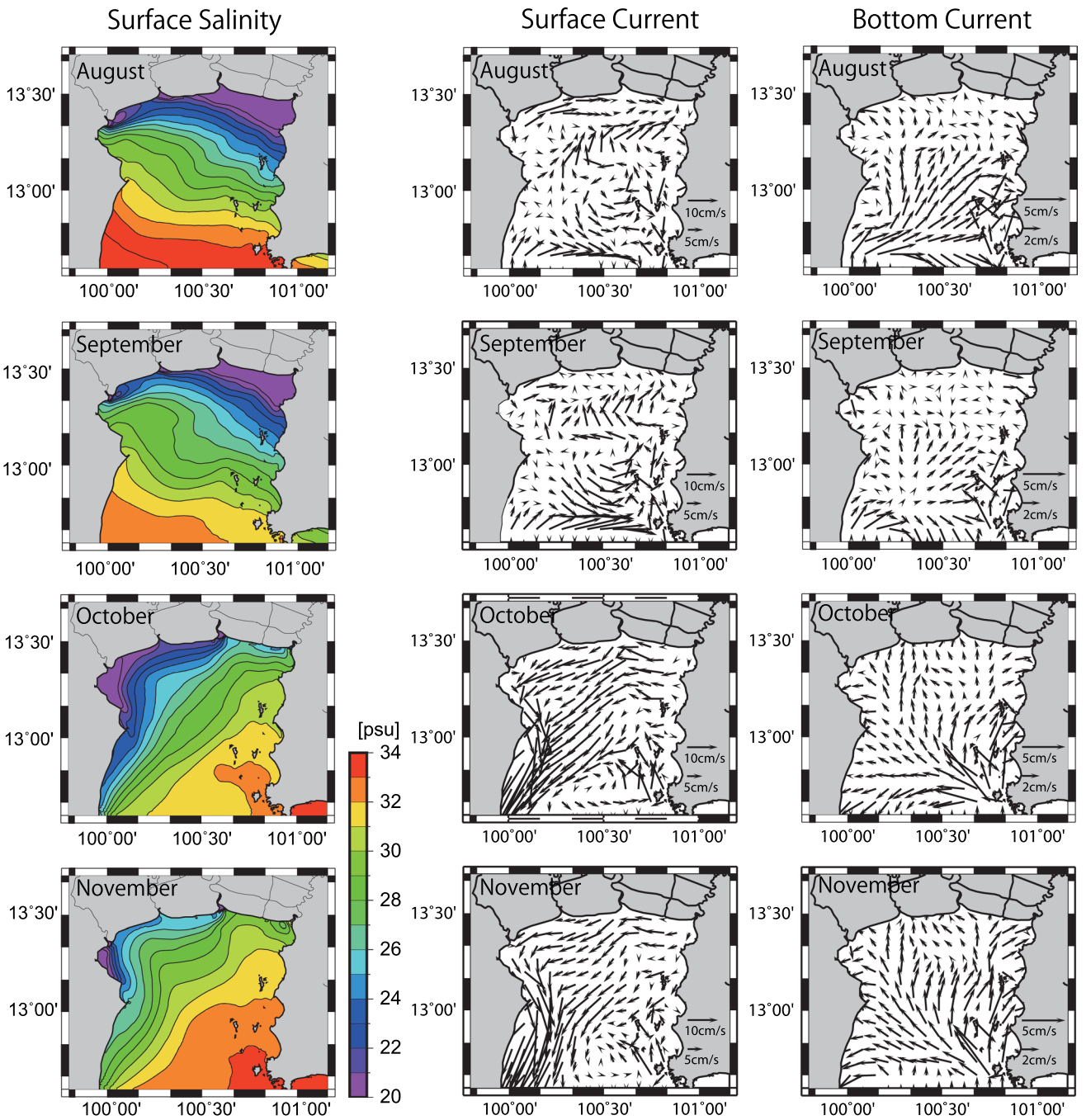


**Fig. 8** Calculated monthly mean of surface salinity and currents at 1 m below the sea surface, and bottom currents at 1 m above the bottom from August to November

in August, but the area of hypoxia expanded to the west. In October, the chlorophyll-*a* distribution was similar to that in September. Hypoxic water masses occupied a large area of the UGoT, and low DO ($< 1$ mg $l^{-1}$) was observed around the mouths of the Bangpakong and Thachin rivers, off Chao-praya and along the western coast. The hypoxic area moved westward from September to October. In November, surface chlorophyll-*a* was high not only along the northern coast, but also along the western coast. In contrast, low chlorophyll-*a* ($< 1$ mg $m^{-3}$) occupied half of the UGoT, where surface salinity was high. A water mass with high salinity and low chlorophyll-*a* intruded into the UGoT from outside the bay on the northward current in the eastern part of the UGoT. The distribution pattern of bottom DO was similar to that in October, but the hypoxic area was smaller. The high-DO water mass expanded to the north in the northeastern part,

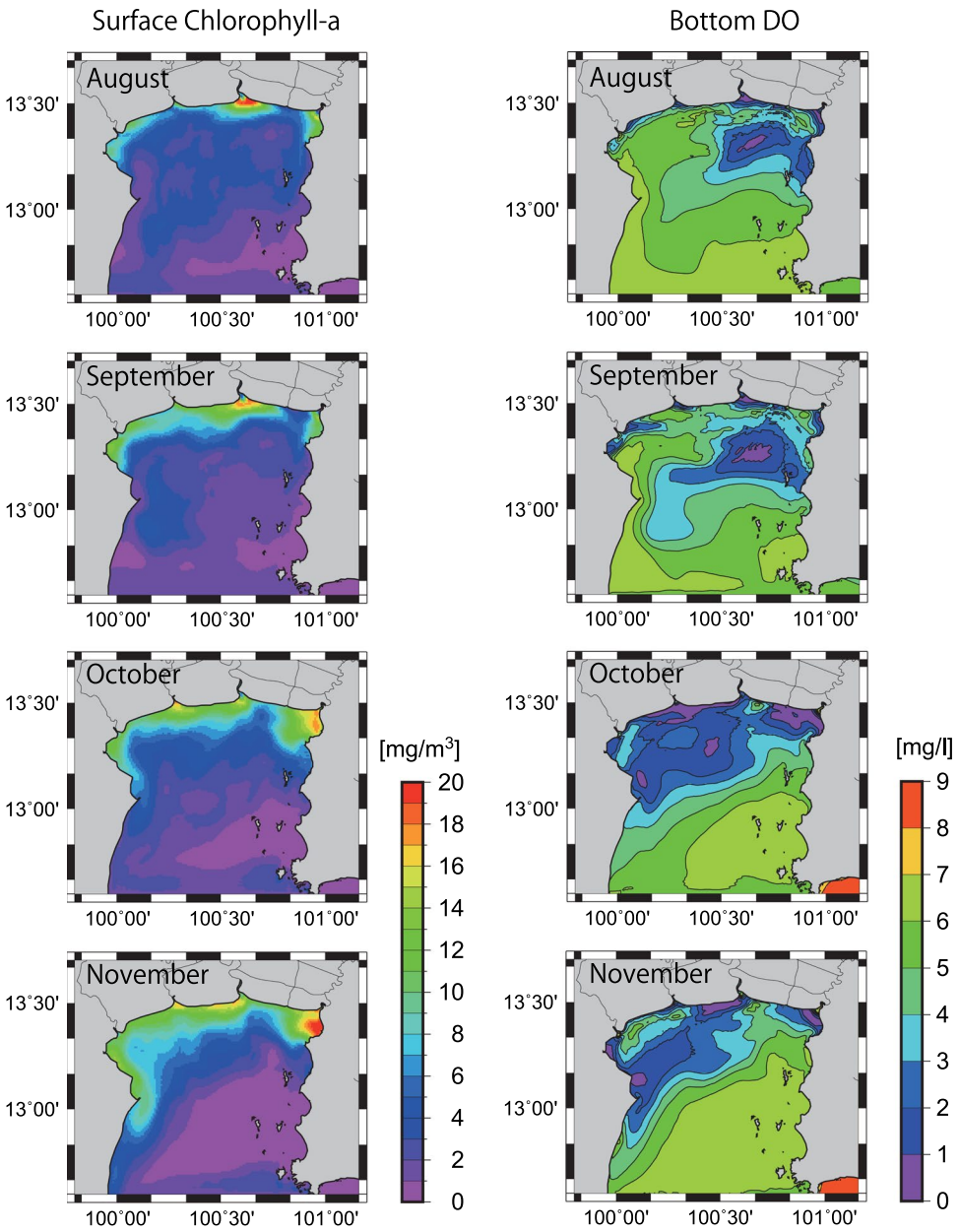


**Fig. 9** Calculated monthly mean of surface chlorophyll-*a* concentration at 1 m below the sea surface and bottom DO concentration at 1 m above the bottom from August to November

and the low-DO water mass expanded to the south along the western coast compared to October.

The hypoxic area moved from the eastern part of the UGoT to the western part from August to November, in accordance with the observations, and the hypoxic area was largest in October.

### 3.3.4 Seasonal variations in the volume of the hypoxic water mass

Figure 10 shows the area-averaged intensity of stratification, calculated using Eq. (1), and the volume of the hypoxic water mass, determined based on the grids where DO was less than 2 mg $l^{-1}$ (integrated across the whole model domain from August 2014 to June 2015). The volume of hypoxia (VHyp) was relatively low in early August, increased by $30\times10^6$ $m^3$ in mid-August, and remained at that level until the end of September. In October, VHyp increased suddenly, reaching a maximum of $110\times10^6$ $m^3$, and high-VHyp conditions persisted until mid-November. VHyp decreased dramatically at the end of November and low VHyp persisted until April. From the end of April, VHyp gradually increased and reached $30\times10^6$ $m^3$ in June.

Comparing VHyp with the area-averaged intensity of stratification (PEA), short time-scale variations were synchronized, while a time lag was present for variations over a long time-scale. The short time-scale variations of PEA corresponded to variations of the spring and neap tide. This

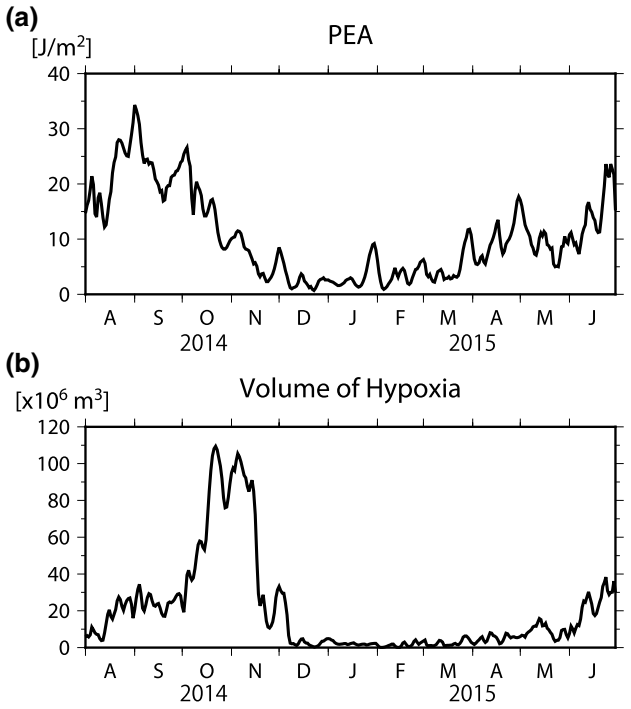


**Fig. 10** Temporal variations in **a** intensity of stratification (PEA) and **b** volume of hypoxia from August 2014 to June 2015

shows that vertical mixing due to tidal currents contributes to the development of hypoxia. Although stratification developed in August and reached its maximum in early September, VHyp was not large in August or September. PEA decreased in late October, but the volume of hypoxic water remained large. In addition, PEA increased from March, while VHyp remained small in March and April.

#### 3.3.5 Causes of hypoxia in three areas

We selected three small areas where hypoxia occurred to investigate how hypoxic water masses are generated (Fig. 1). We focused on the temporal variations of DO concentration in the bottom layer (10th layer of our model). The DO concentration varies due to both physical and biogeochemical processes, as follows.

$$\frac{\partial DO}{\partial t} = \text{Physical process (advection and diffusion)} + \text{Biogeochemical process (photosynthesis, respiration, decomposition)}$$

Hereafter, we examine temporal variations in the values of physical and biogeochemical processes calculated by the model. In addition, to determine the causes of variations in biogeochemical and physical processes, we examine variations in detritus (PON; particulate organic nitrogen) in the bottom layer, vertically integrated chlorophyll-*a* (VIC), and PEA within each small area.

In Area 1, the DO concentration was less than 2 mg $l^{-1}$ from August to mid-September except for a few days; after that, the hypoxic conditions were resolved, except in early October (Fig. 11a). Under the hypoxic conditions in August and September, strong stratification developed (PEA was high, as shown in Fig. 11f) and the PON concentration was elevated (Fig. 11d). The values for the biogeochemical term were all negative, and when the PON concentration was high in mid-August and early to mid-September, the consumption of DO (biogeochemical term) reached about − 1.5 mg $l^{-1}$ $day^{-1}$. VIC varied periodically in August and September, and the biogeochemical term varied with the same periodicity as VIC (Fig. 11c, e). This pattern arises because photosynthesis and respiration induced by phytoplankton vary in the bottom layer, following the variations in VIC. In Area 1, hypoxia occurred in August and September, due to high oxygen consumption driven by an increase of the PON concentration in the bottom layer.

In Area 2, the DO concentration decreased to about 2 mg $l^{-1}$ from August to early September, increased in September and decreased again from the end of September to early October. Relatively low DO conditions (about 2 mg $l^{-1}$) continued through mid-November (Fig. 12a). The physical term had mostly positive values and the biogeochemical term was negative (Fig. 12b, c). The PON concentration was 2–3 μM from August to mid-October, and then gradually increased by 6 μM in early November (Fig. 12d). These variations are reflected in the biogeochemical term: the DO consumption rate due to biogeochemical processes increased from mid-October to early November (Fig. 12c). The biogeochemical term did not show an increasing or decreasing trend from August to mid-October, but short-term variations were observed. On the other hand, the DO concentration varied over a relatively long time scale, with a decreasing trend in August, increasing trend in September, and decreasing trend thereafter. Similar trends occurred for the physical term (Fig. 12b). On the other hand, no such trends were present in PEA from August to mid-October (Fig. 12f). Thus, the vertical supply of DO did not change greatly from August to mid-October. This suggests that the DO concentration in the bottom layer of Area 2 was controlled mainly by horizontal physical processes (advection and diffusion) from August to mid-October. After mid-October, the DO concentration remained low until mid-November, although stratification weakened. During this period,

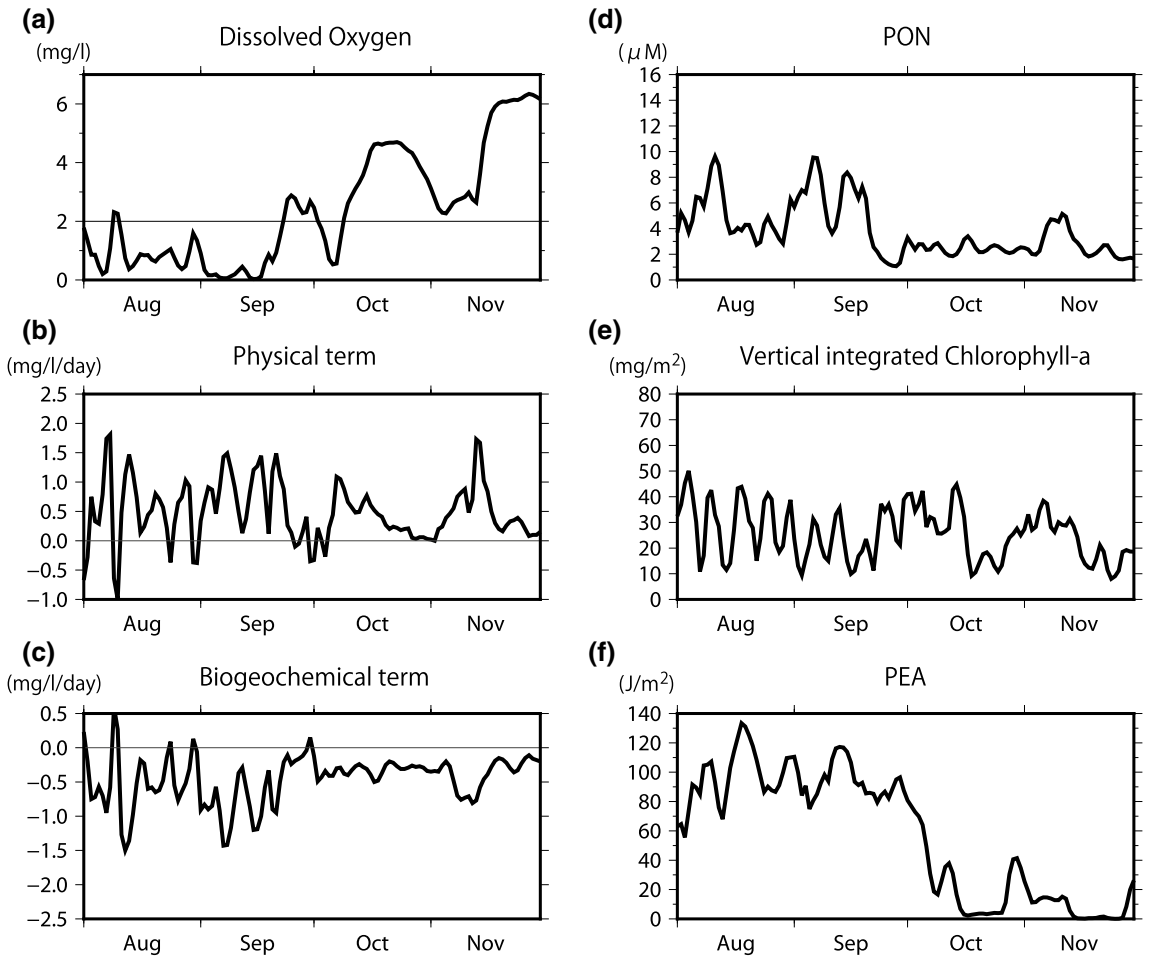


**Fig. 11** Temporal variations in **a** DO concentration in the bottom layer, values of **b** physical term of the model and **c** biogeochemical term related to variability of DO concentration in the bottom layer, **d** PON concentration in the bottom layer, **e** vertical integrated chlorophyll-*a* concentration, and **f** intensity of stratification (PEA) from August to November 2014 in Area-1 shown as red square in Fig. 1 (colour figure online)

low DO was maintained through high DO consumption via biogeochemical processes, while high VIC (Fig. 12e) resulted in high PON (Fig. 12d) in the bottom layer, increasing the DO consumption rate.

In Area 3, the DO concentration was high in August and September and dropped suddenly in late September. Hypoxic conditions continued until the end of November (Fig. 13a). When the DO concentration dropped, PEA increased simultaneously (Fig. 13f). This finding indicates that the development of stratification is related to the occurrence of hypoxia. After stratification had developed, the PON concentration of the bottom layer, VIC, and biogeochemical term all increased (Fig. 13c–e). In addition, the correlation between the PON concentration and biogeochemical term was strong ($r=-0.94$), and that between the VIC and PON concentration (with a 2-day lag) was also strong ($r=0.81$). These findings suggest that the chlorophyll-*a* concentration increased in late September due to the development of stratification; as a result, the PON concentration increased due to the supply of organic matter and the DO consumption rate increased with the decomposition of PON. Therefore, the hypoxia in Area 3 was generated locally.

## 4 Influence of flooding on hypoxia occurrence

Seasonal monsoon rains sometimes cause floods in the Chaopraya River basin. A severe flood occurred in 2011; it was the fifth largest flood in Chaopraya River basin since 1985, with a duration of 158 days (Gale and Saunders 2013). Total discharge from January to May 2011 was similar to that in 2014, but the total discharge in October 2011 (maximum discharge period) was about 3 times larger than in October 2014 (Fig. 4). The total discharge during the dry season (from January to June) of 2012 was about twice as

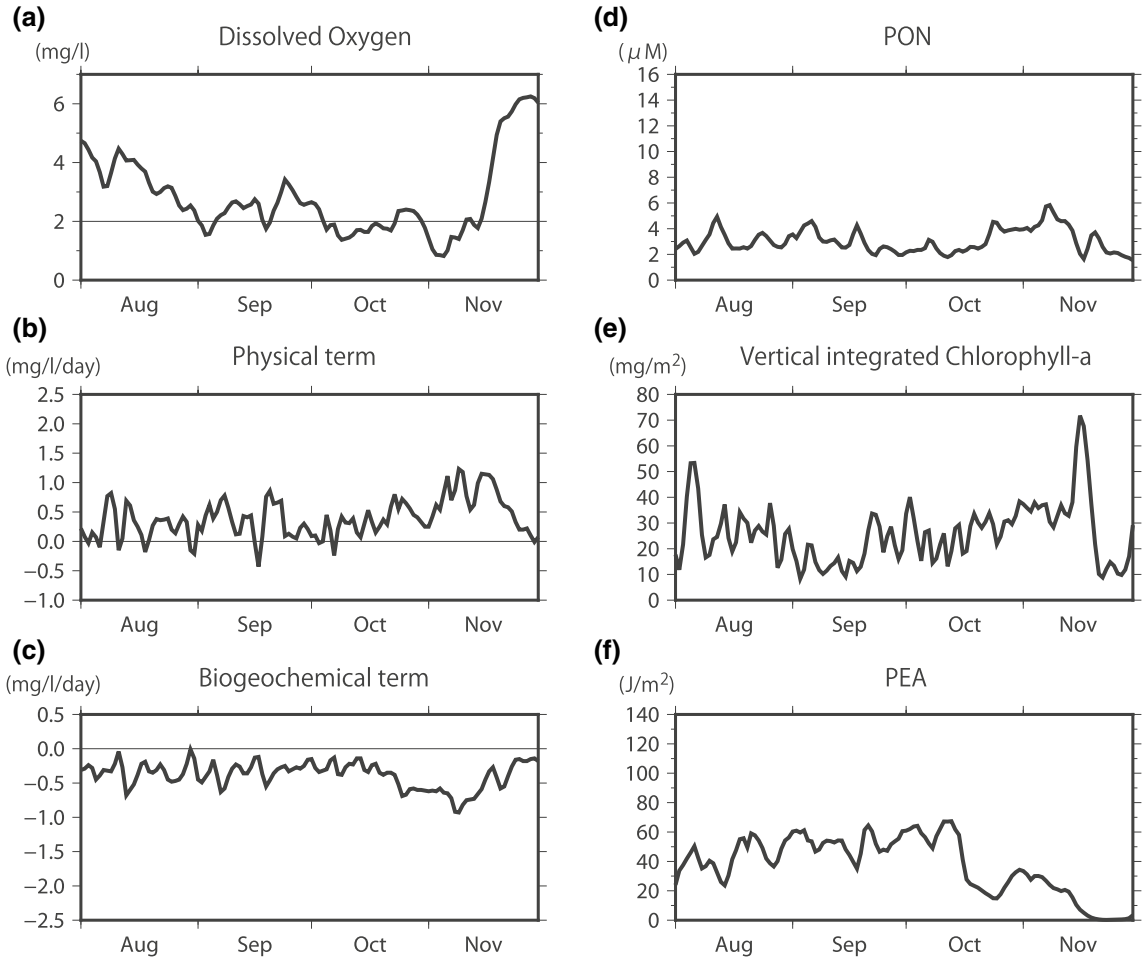


**Fig. 12** Same as Fig. 11 but in Area-2 (colour figure online)

large as in 2015. The total annual freshwater supply (from July to June) in 2011–2012 was $8.3\times10^{10}$ m$^3$, which is 2.6 times greater than the level in 2014–2015 ($3.2\times10^{10}$ m$^3$). A large amount of fresh water was supplied to the UGoT in 2011, allowing a larger hypoxic water mass to develop than in 2014, as stratification was more developed and nutrient inputs were larger. To investigate the effects of such large river discharge on the volume and distribution of hypoxic water in the UGoT, we conducted a numerical experiment. In this experiment, river discharge data from 2011 replaced the corresponding data from 2014, and all boundary and lateral conditions for 2014 were applied. The nutrient concentration in each river was that for 2014–2015. Temporal variations in the intensity of stratification (PEA) and the volume of the hypoxic water mass (VHyp) are shown in Fig. 14. The variation pattern of PEA is similar to that in 2014, but PEA from August to November was about 1.6 times larger in 2011 than in 2014 (Fig. 10a). In addition, PEA from March to June was about 2 times larger in 2012 than in 2014. This suggests that stronger stratification developed not only during the rainy season, but also in the dry season of 2012. The VHyp was much larger in 2011–2012 than in 2014–2015; the maximum volume in October 2011 was $270\times10^6$ m$^3$, about 2.5 times larger than the volume in October 2014. The VHyp became small in December and remained so until mid-March. After that, the VHyp increased until June 2012. The VHyp was $130\times10^6$ m$^3$ in May 2012, which was larger than the maximum volume from 2014 to 2015.

Figure 15 shows the horizontal distributions of bottom DO from August to November 2011. In August 2011, the hypoxic area ($<2$ mg l$^{-1}$) extended further west relative to August 2014, and the low-DO area ($<1$ mg l$^{-1}$) was much larger than in 2014. In September, the low-DO area expanded to the west. In October, the hypoxic area covered half of the UGoT, and low DO was distributed from the northeastern to southwestern part of the UGoT. In November, the distribution of hypoxic area was similar to that in October, but the low-DO area in the eastern part became smaller. The distribution patterns of the hypoxic water mass in the flood year of 2011 were similar to those in 2014.

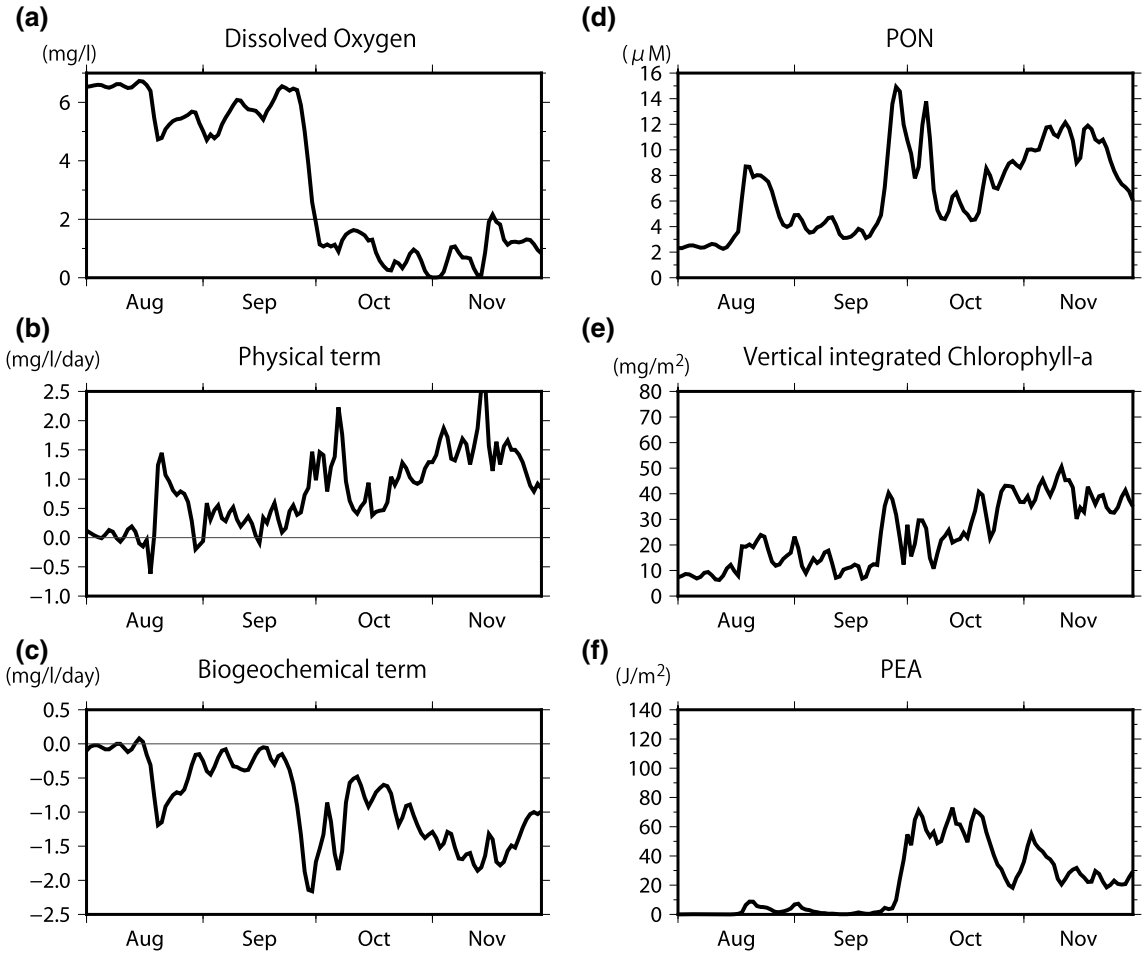


**Fig. 13** Same as Fig. 11 but in Area-3 (colour figure online)

However, severe hypoxic conditions ($< 1$ mg $l^{-1}$) affected a greater area in the flood year of 2011 relative to 2014.

## 5 Discussion and summary

We conducted hydrographic surveys in August, September, November, and December of 2014 and February, April, and June of 2015 to reveal seasonal variations in hypoxic conditions in the UGoT. We found that hypoxia occurs from June to November in the UGoT, and that the hypoxic area moves from east to west seasonally. Low-salinity water, which is diluted river water, also shifts from east to west over time. This pattern occurs because the rotation direction of surface circulation reverses due to a change in the direction of monsoon winds, which are cyclonic in August and September and anti-cyclonic in October and November (Buranapratheprat et al. 2006). As a result of the shift in low-salinity water, the stratified area also moves from east to west. We expected hypoxia to develop in the area of strong stratification. The DO concentration in the bottom layer and the intensity of stratification (PEA) generally showed a negative correlation in September and November. However, hypoxia occurred at a few observation stations despite weak stratification. In addition, the correlation between bottom DO concentration and VAC showed a weak positive correlation in September and a negative correlation in November. Those results suggest that the low-DO water mass is not generated at the observation point, and is instead transported on currents past multiple stations.

We developed a physical-ecosystem model to reproduce the shifts of hypoxic and low-salinity water masses and investigated the temporal and spatial variations of hypoxia in the UGoT. The shift of low-salinity water and the hypoxic area from east to west was reproduced well by the model. According to the modeling result, the VHyp in the UGoT reaches a maximum in October (Fig. 10b), although we did not conduct hydrographic observations in October. This result might be driven by river discharge, which was largest in October (Fig. 4a), and by an area of high chlorophyll-*a* covering the northern part of the UGoT (Fig. 9). This peak in river discharge leads to the strongest stratification and

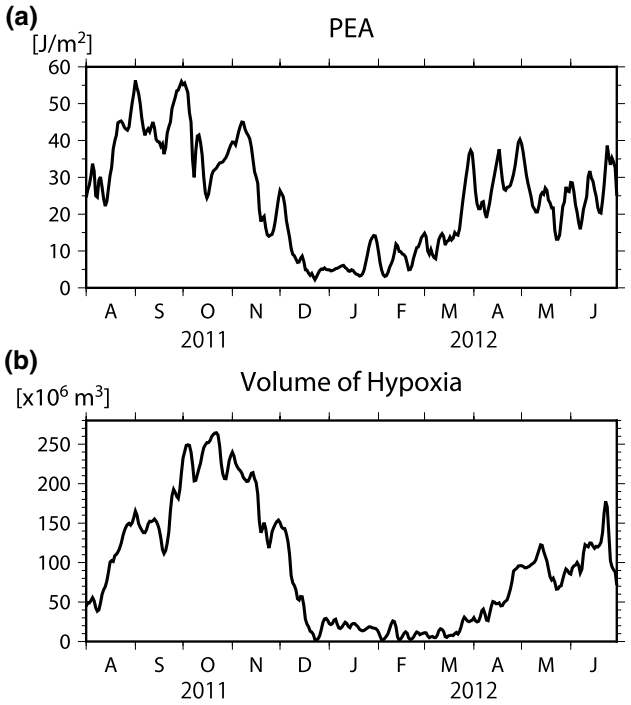


**Fig. 14** Temporal variations in **a** intensity of stratification (PEA) and **b** volume of hypoxia from August 2011 to June 2012 when severe flood occurred in Chaopraya basin

supplies large amounts of nutrients. As a result, the chlorophyll-*a* concentration increases across a wide area, and a large amount of organic matter sinks to the bottom, where the DO consumption rate increases due to biogeochemical processes (decomposition), and vertical DO supply due to physical processes decreases due to strong stratification.

We investigated the temporal variations in bottom DO, DO consumption rate, and PEA in three areas where hypoxia occurs. In Areas 1 and 3, the hypoxic water mass is generated locally, while in Area 2, the low-DO water mass is transported from the surrounding area. Figure 16 shows the monthly average bottom DO consumption rate (biogeochemical term in the model) from August to November 2014. The DO consumption rate is high in each estuarine region and offshore of the Chaopraya and Bangpakong rivers. The region of high DO consumption shifts westward during this season. The distribution patterns of surface chlorophyll-*a* shown in Fig. 9 are similar to the pattern of the DO consumption rate. Increasing vertical flux of organic matter results in high DO consumption in the bottom layer.

Flooding supplies a great deal of freshwater and nutrients to the UGoT and might cause strong stratification and blooms of phytoplankton. Therefore, hypoxia is considered likely to develop after floods. Severe flooding occurred in 2011. To explore the influence of flooding on the intensity of hypoxia, we conducted a simulation using river discharge data from 2011 and 2012. The volume of hypoxic water was 2.5 times larger in 2011 than 2014, and the hypoxic water mass was also present in the dry season of 2011. After flooding occurred in the Chaopraya River basin, river discharge did not decrease for a long time (Fig. 4b) due to the gentle gradient of the Chaopraya River basin. Therefore, the influence of flooding on the marine environment continues into

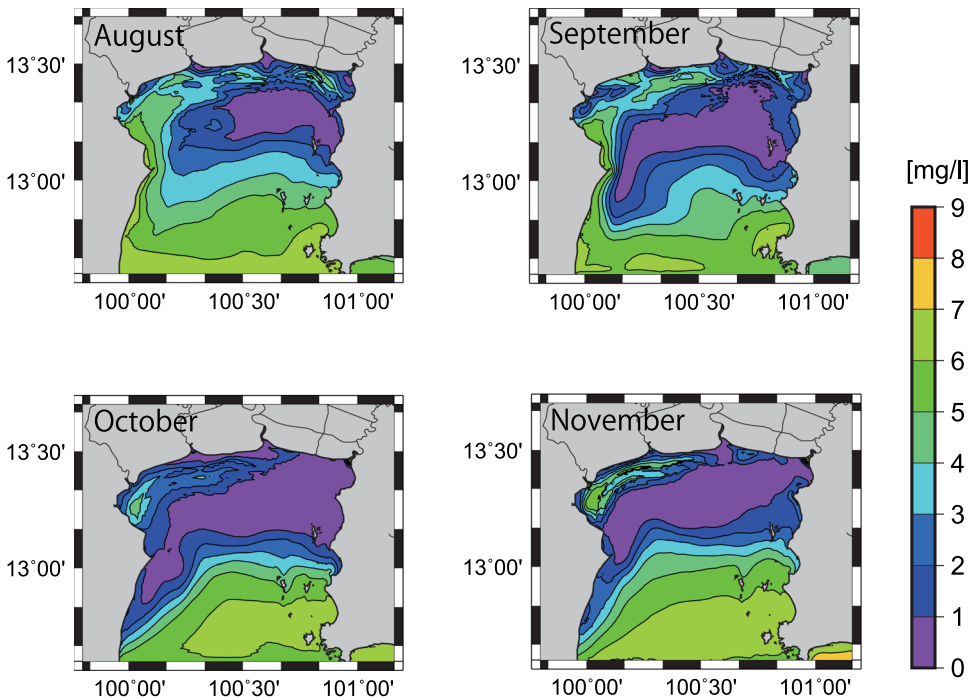


**Fig. 15** Horizontal distribution of monthly mean of DO concentration at 1 m above the bottom from August to November in 2011

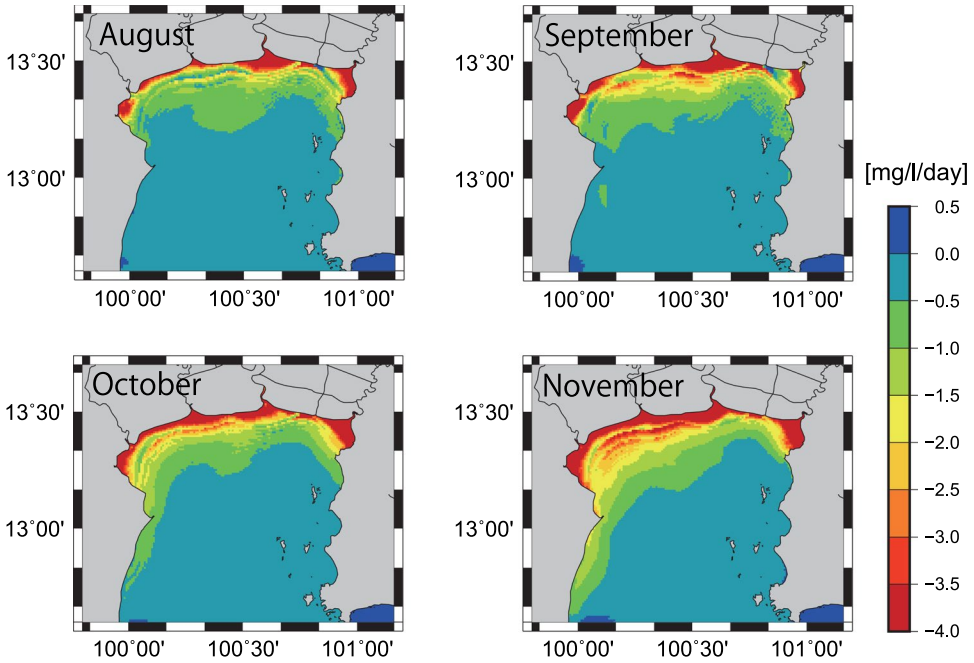


**Fig. 16** Horizontal distribution of monthly mean of DO consumption rate at 1 m above the bottom from August to November 2014

the following year, driving hypoxia in April and May 2011, as shown in Fig. 14. As hypoxic conditions persist for a long time during flood years, dramatic decreases in the abundance of benthic organisms are likely.

Nutrient concentrations in rivers around the UGoT were high; our observational data show that the maximum DIN concentrations of the Chaopraya and Thachin rivers are 245 and 300 µM, respectively. A red tide of *Noctiluca* occurs offshore of the Chaopraya and Bangpakong rivers annually (Lirdwitayaprasit et al. 2006). Enormous amounts of organic matter may accumulate in the bottom sediment, releasing nutrients. Even with a reduction of nutrient fluxes from rivers through improved sewage treatment, hypoxia is likely to persist for a long time in the UGoT. Nutrient management is essential to protect the marine environment of the UGoT.

**Acknowledgements** We appreciate captain and crews of research vessel of Kasetsart University and students in Department of Aquatic Science, Faculty of Science, Burapha University for their help during hydrographic observations. This research was financially supported by the Japan Society for the Promotion of Science, Grant-in-Aid for Scientific Research (B) (26302001) and is partially supported by JSPS Core-to-core CREPSUM JPJSCCB20200009.

## References

Altieri AH, Gedan KB (2015) Climate change and dead zones. Glob Change Biol 21:1395–1406. https://doi.org/10.1111/gcb.12754

Blumberg AF, Mellor GL (1987) A description of a three dimensional coastal ocean circulation model. In: Heaps N (ed) Three-dimensional coastal ocean models, Coastal estuarine stud. 4. AGU, Washington, pp 1–16 (**208 pp**)

Breitburg D, Levin LA, Oschlies A, Gregoire M, Chavez FP, Conley DJ, Garcon V, Gilbert D, Gutierrez D, Isensee K, Jacinto GS, Limburg KE, Montes I, Naqvi SWA, Pitcher GC, Rabalais NN, Roman MR, Rose KA, Seibel BA, Telszewski M, Yasuhara M, Zhang J (2018) Declining oxygen in the global ocean and coastal waters. Science 359(6371):eaam7240

Buranapratheprat A, Yanagi T, Sawangwong P (2002) Seasonal variations in circulation and salinity distributions in the Upper Gulf of Thailand: Modeling approach. La Mer 40:147–155

Buranapratheprat A, Yanagi T, Sojisuporn P, Booncherm C (2006) Influence of local wind field on seasonal circulation in the Upper Gulf of Thailand. Coast Mar Sci 30(1):19–26

Buranapratheprat A, Yanagi T, Matsumura S (2008a) Seasonal variation in water column conditions in the upper Gulf of Thailand. Cont Shelf Res 28:2509–2522

Buranapratheprat A, Yanagi T, Niemann OK, Matsumura S, Sojisuporn P (2008b) Surface chlorophyll-a dynamics in the Upper Gulf of Thailand revealed by a coupled hydrodynamic-ecosystem model. J Oceanogr 64:639–656

Buranapratheprat A, Niemann KO, Matsumura S, Yanagi T (2009) MERIS imageries to investigate surface chlorophyll in the upper Gulf of Thailand. Coast Mar Sci 33(1):22–28

Capet A, Beckers J-M, Gregoire M (2013) Drivers, mechanisms and long-term variability of seasonal hypoxia on the Black Sea northwestern shelf—is there any recovery after eutrophication? Biogeosciences 10:3943–3962

Carstensen J, Andersen JH, Gustafsson BG, Conley DJ (2014) Deoxygenation of the Baltic Sea during the last century. Proc Natl Acad Sci USA 111(15):5628–5633

Cheevaporn V, Menasveta P (2003) Water pollution and habitat degradation in the Gulf of Thailand. Mar Poll Bull 47:43–51

Chongprasith P, Srineth V (1998) Marine water quality and pollution of the Gulf of Thailand. In: DM Johnston (ed) SEAPOL Integrated Studies of the Gulf of Thailand, vol 1. Southeast Asian Programe in Oecan Law, Policy and Management. pp 137–204

Diaz RJ (2001) Overview of hypoxia around the world. J Environ Qual 30:275–281

Diaz RJ, Rosenberg R (2008) Spreading dead zones and consequences for marine ecosystem. Science 321:926–929

Gale EL, Saunders MA (2013) The 2011 Thailand flood: climate causes and return periods. Weather 68(9):233–237

Hayami Y, Morimoto A, Sudaryanto A, Sachoemar IS, Soeyanto E, Rusdiansyah A, Saleh M (2020) A quasi-persistent hypoxic water mass in an equatorial coastal sea, Jakarta Bay, Indonesia. Est Coast Shelf Sci. 246:107030

Jacinto GS, Sotto LPA, Senal MIS, San Diego-McGlone ML, Escobar MTL, Amano A, Miller TW (2011) Hypoxia in Manila Bay, Philippines during the northeast monsoon. Mar Poll Bull 63:243–248

Kemp WM, Testa JM, Conley DJ, Gilbert D, Hagy JD (2009) Temporal responses of costal hypoxia to nutrient loading and physical controls. Biogeosciences 6:2985–3008

Kim H, Takayama K, Hirose N, Onitsuka G, Yoshida T, Yanagi T (2019) Biological modulation in the seasonal variation of dissolved oxygen concentration in the upper Japan Sea. J Oceanogr 75:257–271

Li M, Lee YJ, Testa JM, Li Y, Ni W, Kemp WM, Toro DMD (2016) What drives interannual variability of hypoxia in Chesapeake Bay: climate forcing versus nutrient loading? J Res Lett 43:2127–2134. https://doi.org/10.1002/2015GL067334

Lirdwitayaprasit T, Meksumpun S, Rungsupa S, Furuya K (2006) Seasonal variations in cell abundance of *Noctiluca scintillans* in the coastal waters off Chonburi Province, the Upper Gulf of Thailand. Coast Mar Sci 30(1):80–84

Mellor GL (2003) User guide for a three-dimensional, primitive equation, numerical ocean model (2003 version) (report, 53 pp). Program in Atmosphere and Ocean Science. Princeton Univ., Princeton

Mellor GL, Yamada T (1982) Development of a turbulence closure model for geophysical fluid problems. Rev Geophys 20:851–875

Morimoto A, Buranapratheprat A, Kaneda A, Sunitsakul S, Jintasaeranee P, Gunboa V, Tomita H (2013) Behavior of anoxic water in the Bangpakong estuary. Mar Res Indones 37(2):109–121

Nakajima M, Fujiwara T (2007) Estuarine circulation and hypoxic water mass in Osaka Bay. Bull Coast Ocenogr 44(2):157–163 (**in Japanese with English abstract**)

Onitsuka G, Yanagi T, Yoon J-H (2007) A numerical study on nutrient sources in the surface layer of the Japan Sea using a coupled physical-ecosystem model. J Geophys Res 112:C05042. https://doi.org/10.1029/2006JC003981

Rabalais NN, Turner RE (2019) Gulf of Mexico Hypoxia: past, present, and future. Limno Oceanogr Bull. https://doi.org/10.1002/lob.10351

Sotto LPA, Jacinto GS, Villanoy CL (2014) Spatiotemporal variability of hypoxia and eutrophication in Manila Bay, Philippines during the northeast and southwest monsoons. Mar Poll Bull 85:446–454

Smagorinsky JS (1963) General circulation experiments with the primitive equations. I. The basic experiment. Mon Weather Rev 91:99–164

Tong-U-Dom S, Na-U-Dom T, Buranapratheprat A (2017) The responses of a hydrodynamic model to different open boundary conditions in the Northern Gulf of Thailand. Burapha Sci J 22(3):259–272 (**in Thai with English abstract**)

Yanagi T, Yamada M (2014) Disappearance of hypoxia in Dokai Bay. Japan Bull Coast Ocenogr 51(2):203–208

Yu X, Guo X, Morimoto A, Buranapratheprat A (2018) Simulation of river plume behaviors in a tropical region: case study of the Upper Gulf of Thailand. Cont Shelf Res 153:16–29